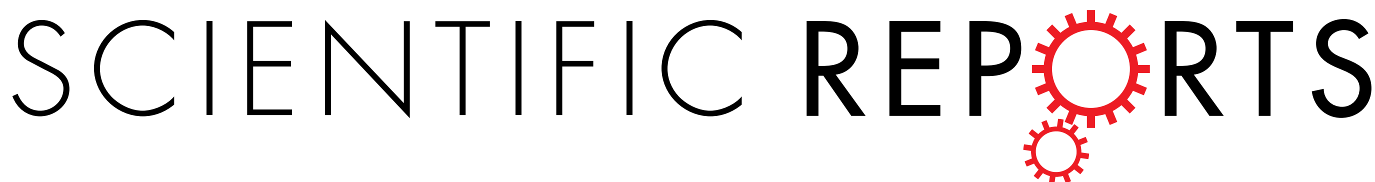

OPEN

Self-Limiting Layer Synthesis of Transition Metal Dichalcogenides

Youngjun Kim[1,*], Jeong-Gyu Song[1,*], Yong Ju Park[1], Gyeong Hee Ryu[2], Su Jeong Lee[3], Jin Sung Kim[4], Pyo Jin Jeon[4], Chang Wan Lee[1], Whang Je Woo[1], Taejin Choi[1], Hanearl Jung[1], Han-Bo-Ram Lee[5], Jae-Min Myoung[3], Seongil Im[4], Zonghoon Lee[2], Jong-Hyun Ahn[1], Jusang Park[1] & Hyungjun Kim[1]

Received: 11 May 2015
Accepted: 18 November 2015
Published: 04 January 2016

This work reports the self-limiting synthesis of an atomically thin, two dimensional transition metal dichalcogenides (2D TMDCs) in the form of MoS_2. The layer controllability and large area uniformity essential for electronic and optical device applications is achieved through atomic layer deposition in what is named self-limiting layer synthesis (SLS); a process in which the number of layers is determined by temperature rather than process cycles due to the chemically inactive nature of 2D MoS_2. Through spectroscopic and microscopic investigation it is demonstrated that SLS is capable of producing MoS_2 with a wafer-scale (~10 cm) layer-number uniformity of more than 90%, which when used as the active layer in a top-gated field-effect transistor, produces an on/off ratio as high as 10^8. This process is also shown to be applicable to WSe_2, with a PN diode fabricated from a MoS_2/WSe_2 heterostructure exhibiting gate-tunable rectifying characteristics.

Two-dimensional (2D) materials, and the heterostructures that can be created from them, have been widely studied due to their atomic-scale thickness, flexibility and unique electrical/optical properties[1–5]. However, there is still a need to develop a layer-controlled synthesis method capable of producing a uniform 2D material over large areas in order to ensure the reliable operation of optoelectronic devices whose properties are dependent on the number of 2D material layers. The well-established CVD process has allowed large-area graphene sheets to be used in various practical applications[6,7], as this process is self-limited through a surface-catalyzed process based on the lower solubility of carbon in Cu than in Ni[8]. Since it is this self-limiting behavior that makes it possible to achieve monolayer (1L) graphene over 95% of the target growth area[8], achieving a similar self-limiting behavior is clearly an important first step in the development of any new process for the large-area uniform growth of 2D materials.

Transition metal dichalcogenides (TMDCs) and their relevant 2D heterostructures (e.g., MoS_2/WSe_2 and MoS_2/graphene) have been the most heavily studied semiconducting 2D materials[3,4,9–13]. Most recent research has been devoted to synthesizing uniform and layer-controlled TMDCs over large areas[9,14,15], such as chemical vapor deposition and transformation of Mo and MoOx thin film[16,17,18], but unlike graphene, the self-limiting growth of TMDCs with wafer-level layer controllability and uniformity has not yet been achieved. Atomic layer deposition (ALD) is known to be self-limiting, as the growth rate is dependent on the adsorption of precursor molecules rather than growth conditions such as exposure time[19,20], but as growth occurs through the formation of multi-layer islands it is difficult to achieve the layer controllability needed when compared to other techniques such as CVD[21,22]. Maximizing the self-limiting behavior of the ALD process is therefore essential to achieving the layer controllability needed for a 2D structure, which requires not only careful optimization of the process conditions (e.g., temperature, pressure, exposure of precursor/reactant), but also the careful selection of the precursor and reactant[23,24]. Moreover, since the ALD process is entirely based on surface reaction, it is important to understand the surface characteristics of the material being deposited. For example, the ALD of metal oxides or metals on graphene is made difficult by the chemically inactive nature of the graphene surface[25–27]. As 2D TMDCs also have a chemically inactive surface, it is reasonable to expect they will exhibit a unique growth behavior during ALD when compared to conventional materials that are rich in dangling bonds[28].

[1]School of Electrical and Electronic Engineering, Yonsei University, Seoul 120-749, Korea. [2]School of Materials Science and Engineering, Ulsan National Institute of Science and Technology (UNIST), Ulsan 689-798, Korea. [3]Department of Materials Science and Engineering, Yonsei University, Seoul 120-749, Korea. [4]Institute of Physics and Applied Physics, Yonsei University, Seoul 120-749, Korea. [5]Department of Materials Science and Engineering, Incheon National University, Incheon 406-772, Korea. [*]These authors contributed equally to this work. Correspondence and requests for materials should be addressed to H.K. (email: hyungjun@yonsei.ac.kr)

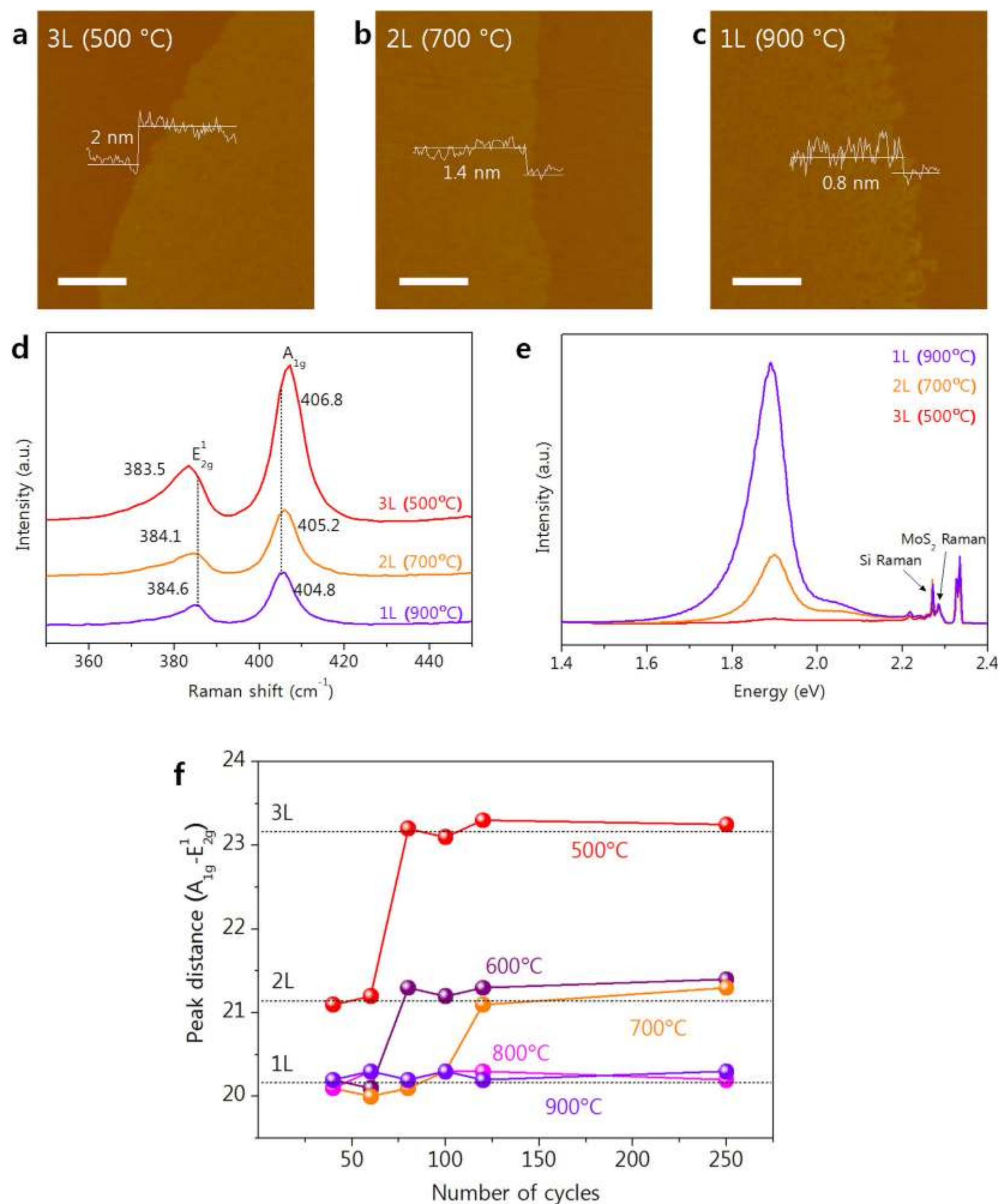

Figure 1. AFM images and height profiles of (**a**) tri-, (**b**) bi- and (**c**) mono-layers of MoS_2 transferred onto a SiO_2 substrate (scale bar = 0.5 μm).(**d**) Raman spectra and (**e**) PL spectra of tri-, bi- and mono-layer MoS_2 on SiO_2. (**f**) Raman peak distances for MoS_2 with various SLS cycles and growth temperatures.

In this study, the self-limiting layer synthesis (SLS) of a 2D TMDC (MoS_2) is achieved through ALD by combining precursor exposure, purging, reactant exposure and a final purging into a single cycle. In this way, a point is reached at which the number of layers produced is determined purely by the growth temperature; a unique behavior that is directly attributable to the chemical inactivity of the 2D MoS_2 surface. The characteristics and layer uniformity achieved are subsequently assessed through spectroscopic and microscopic analysis, and the universality of the process itself is tested by applying it to the fabrication of a MoS_2/WSe_2 heterostructure for use in a diode.

Self-limiting layer synthesis of MoS_2

Figure 1(a–c) contains AFM images and height profiles of MoS_2 synthesized through 120 ALD cycles at growth temperatures of 500, 700 or 900 °C. By transferring this MoS_2 to new SiO_2 substrates it was found that the thickness produced was 2 nm at 500 °C, 1.4 nm at 700 °C and 0.8 nm at 900 °C, which corresponds to the thickness of tri-, bi-, and mono-layer (3L, 2L, and 1L) MoS_2[29]. The Raman spectra ($\lambda_{exc} = 532$ nm) in Fig. 1(d) shows that the 1L MoS_2 exhibits E^1_{2g} and A_{1g} modes from in-plane and out-of-plane vibrations at 384.6 cm^{-1} and 404.8 cm^{-1}, but these shift to 384.1 and 405.2 cm^{-1} with 2L MoS_2, and to 383.5 and 406.8 cm^{-1} with 3L MoS_2. The peak distance between

E^1_{2g} and A_{1g} is often used to determine the number of MoS_2 layers, as an increase in layers is accompanied by a softening of the E^1_{2g} mode frequency and a stiffening of the A_{1g} mode frequency[30,31]. In this case, the calculated peak distances of 20.2 cm^{-1} for 1L, 21.1 cm^{-1} for 2L, and 23.3 cm^{-1} for 3L all agree well with previously reported values for MoS_2[29,32,33]. Thus, both the AFM and Raman results show that it is the growth temperature that determines the number of MoS_2 layers by SLS.

The PL spectra of the synthesized MoS_2 are shown in Fig. 1(e) as a function of the number of layers obtained. Note that the 1L MoS_2 spectrum exhibits a strong PL signal at 1.89 eV and a weak, wide PL signal at 2.05 eV, which correspond to the A_1 and B_1 direct excitonic transitions of MoS_2[14,34]. These signals weaken in the case of 2L MoS_2, and become negligible with 3L MoS_2, as the increasing number of layers induces a transition from a direct to an indirect band gap. This is concordant with previous results regarding the dependence of the PL signal on the number of layers[14,34,35] and further confirms the growth temperature dependent nature of the SLS of MoS_2.

Given the good correlation between the Raman peak distances and the number of layers of MoS_2 obtained on a SiO_2 substrate, this was used a criterion to assess the effects of varying the number of process cycles from 40 to 250 at growth temperatures of 500, 600, 700, 800 and 900 °C (the Raman spectra for each point are presented in Supplementary Fig S2). From the results shown in Fig. 1(f), it is evident that the number of MoS_2 layers does not increase linearly with the number of process cycles, but rather saturates at a certain critical point determined by the synthesis temperature (500 °C for 3L, 600–700 °C for 2L, and 800–900 °C for 1L). This stands in stark contrast to conventional ALD, in which the thickness does in fact increase linearly with the number of process cycles. We can therefore only conclude that the growth mechanism of the current SLS process is totally different from that of conventional ALD.

This peculiar "self-limiting" behavior of ALD during the SLS process is believed to be caused by the inherently chemically inactive nature of the surface of TMDCs such as MoS_2. Specifically, during the growth of the first layer, precursor molecules ($MoCl_5$ in this case) chemically adsorb to the abundant adsorption sites on the SiO_2 surface. However, once this initial layer is formed over the entire surface, any further chemical adsorption of precursor molecules is hindered by the absence of suitable adsorption sites on the newly created TMDC surface[28,36]. Synthesis is therefore forced to proceed through the physical adsorption of $MoCl_5$ molecules on MoS_2; with the adsorption/desorption of precursor molecules under this physical adsorption-dominant regime being determined by the growth temperature. This can perhaps be better explained by the framework of the Lennard-Jones potential model: i.e., at lower temperatures molecules are trapped in a potential well because their thermal energy is less than the potential depth, whereas at higher temperatures they have sufficient thermal energy to escape[28,36].

The surface potential of MoS_2 that is induced by the positive charge between it and the SiO_2 substrate also affects the potential depth of the precursor molecules; the surface potential of MoS_2 decreasing with an increasing number of MoS_2 layers due to their screening effect on the electric field[37]. This decrease in surface potential can reduce the potential depth of the $MoCl_5$ molecule on MoS_2 in the same way that the surface potential of physically adsorbed CH_4 on h-BN decreases with an increasing number of layers[38]. In other words, once a specific number of MoS_2 layers has been formed at any given growth temperature, any $MoCl_5$ molecules adsorbed onto the MoS_2 basal plane can be easily desorbed due to the reduced potential depth, thereby creating a self-limiting growth behavior.

It should be noted here that the SLS of 2D MoS_2 relies on using a sufficiently high process temperature to ensure the formation of layered 2D structure with chemically inactive surface. The lower crystallinity and non-layered 3D structure at lower growth temperatures causes deposition to proceed through chemical adsorption of precursor molecules, as is the case in the conventional ALD of MoS_2 without self-limiting growth behavior[21,22]. These temperature requirements make proper selection of the precursor essential, with $MoCl_5$ being used in this study due to its higher thermal stability relative to other metal organic precursors.

The uniformity of the MoS_2 obtained through SLS was evaluated at different scales through Raman mapping of the peak distances between the A_{1g} and E^1_{2g} modes. The Raman map of the 1L SLS MoS_2 in Fig. 2(a) shows a perfectly uniform distribution at a micrometer scale (20 μm × 20 μm), with statistical analysis (see Supplementary Fig. S6) revealing the average peak distance and standard deviation to be 20.3 and 0.6, respectively. Uniformity at a wafer-level scale was measured by synthesizing 1L, 2L and 3L MoS_2 onto 1.5 × 9 cm^2 SiO_2 substrates; the substrate size being limited in this instance by the diameter (~3 cm) and length (15 cm hot zone) of the tube furnace used. It is clear from Fig. 2(b) that the color of the SLS MoS_2 is certainly dependent on the number of layers, but to assess the cm-scale uniformity, Raman spectra were measured at nine different positions along the length of the SLS MoS_2. The peak distances and full-width at half-maximum (FWHM) of the E^1_{2g} and A_{1g} modes are plotted in Fig. 2(c) for each position, from which we see that with all samples the variation in peak distance and FWHM of the E^1_{2g} and A_{1g} modes with position is quite small (~2% for peak distance, ~5 and ~4% for the FWHM of E^1_{2g} and A_{1g}, respectively). In addition, the Raman peak distance varies from 20.2 to 23.4 cm^{-1} as the number of layers is increased, confirming that good uniformity and layer control is achieved at the wafer level through the SLS of MoS_2.

The crystallinity and electrical performance of the 1L SLS MoS_2 was evaluated through high-resolution TEM (HRTEM) analysis and by using it in a top-gated field-effect transistor (FET). The low-magnification TEM image of 1L SLS MoS_2 in Fig. 2(d) reveals triangular, dark-contrast regions of 2L MoS_2; but as these represent only about 4% of the total area, the 1L SLS MoS_2 can be considered to have near-perfect ($>$ 95%) micrometer-scale layer uniformity. This growth of 2L MoS_2 on 1L MoS_2 could be due to the energetically favorable adsorption of $MoCl_5$ on defect sites such as sulfur vacancies or grain boundaries, as such adsorption of molecules is seen with graphene[26,27]. In the HRTEM image of the 1L SLS MoS_2 in Fig. 2(e), selected regions exhibit a honeycomb-like with a lattice spacing of 0.27 or 0.16 nm depending on whether it involves (100) or (110) planes. A six-fold coordination symmetry is also clearly evident in the fast Fourier transform (FFT) image in the inset of Fig. 2(e). The approximate grain size is 80–100 nm, though this could potentially be improved through further optimization of the process and substrate conditions. The electrical performance of the 1L SLS MoS_2 was evaluated by using it in the fabrication of a top-gated FET with Au(10 nm)/Ti(50 nm) electrodes and an ALD Al_2O_3 (40nm) gate insulator. The room temperature performance of this FET at 10^{-5} mTorr is shown in Fig. 2(f), which reveals an n-type behavior; the

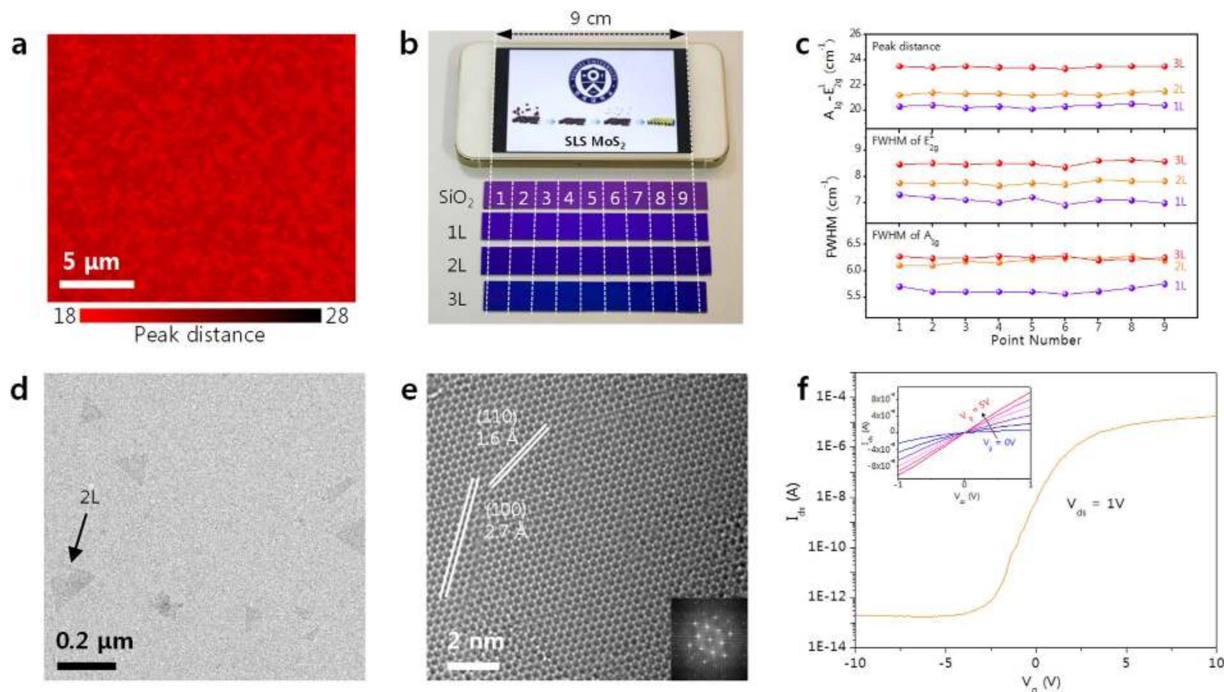

Figure 2. (**a**) Raman map of peak distance between E^1_{2g} and A_{1g} modes for monolayer MoS_2 (scale bar = 5 μm). (**b**) Large-area (~9 cm) mono-, bi-, and tri-layer MoS_2 on a SiO_2 substrate comparable in size to a cellular phone display screen. (**c**) Relative peak distances and FWHM of E^1_{2g} and A_{1g} modes for nine measurement points on mono-, bi-, and tri-layer MoS_2. (**d**) Low-magnification TEM image (scale bar = 0.2 μm) of monolayer MoS_2 on a TEM grid and (**e**) HRTEM image (scale bar = 2 nm) of the selected region. The inset gives the corresponding FFT pattern. (**f**) Transfer curve and (inset) output curve for a FET fabricated on monolayer MoS_2.

0.2 $cm^2/V{\cdot}s$ field effect electron mobility in the linear regime of the transfer curve agreeing with a previous report of a MoS_2 FET[39]. Interestingly, this 1L SLS MoS_2 FET also has a low subthreshold swing value of ~0.36 V/dec and an excellent on/off current ratio of ~10^8 that is higher than anything previously achieved with 1L MoS_2[18], and is in fact comparable with a single crystal[39].

Vertically stacked heterostructure. If the proposed self-limiting growth mechanism of SLS is valid, then it would be expected to apply to other 2D materials. This was therefore tested using mechanically exfoliated WSe_2 flakes on a SiO_2(300 nm)/Si substrate, as demonstrated by the microscopy (OM) images in Fig. 3(a). This WSe_2 flake was confirmed through AFM and Raman analysis (See Supplementary Fig. S8(a–c)) to contain regions of both 2L WSe_2 (#2) and 12L WSe_2 (#3). The AFM image of the SLS MoS_2 produced on this WSe_2 flake at 800 °C (Fig. 3(b)) shows that a thickness of 1.3 nm (or 2L WSe_2) was obtained, indicating that 1L MoS_2 is deposited on both 2L WSe_2 and the SiO_2 substrate under these conditions. Figure 3(c) shows the Raman spectra obtained at 3 different points of the SLS MoS_2 on WSe_2/SiO_2. In the SiO_2 region (#1), E^1_{2g} and A_{1g} Raman peaks for MoS_2 are observed at 385.2 and 405 cm^{-1}, respectively, with the peak distance of 20.2 indicating that 1L MoS_2 was obtained as expected. Raman peaks of WSe_2 (i.e., the sum of the E^1_{2g} and A_{1g} peaks at 249.8 cm^{-1}) are observed in the 2L WSe_2 region (#2) along with peaks for MoS_2 (E^1_{2g} at 378.4 cm^{-1} and A_{1g} at 404.8 cm^{-1}), indicating that MoS_2 was also synthesized on the WSe_2 flake. Furthermore, the absence of any Raman peaks related to $MoSe_2$ (E^1_{2g} at 286 cm^{-1} and A_{1g} at 244 cm^{-1}) or WS_2 (E^1_{2g} at 356 cm^{-1} and A_{1g} at 420 cm^{-1}) indicates that there is no significant mixing or alloying between the two 2D materials[15,40]. There is, however, a notable 7 cm^{-1} downshift in the E^1_{2g} peak of MoS_2 in the 1L MoS_2/WSe_2 region relative to the MoS_2/SiO_2 region. A similar downshift has been reported in the case of an interlayer-coupled 1L MoS_2/1L WSe_2 heterostructure fabricated by transferring individual MoS_2 and WSe_2 flakes, with this being attributed to interaction between MoS_2 and WSe_2[41]. Meanwhile, the absence of any MoS_2 Raman peaks in the 12L WSe_2 (#3) region indicates that there is effectively no growth of MoS_2 on 12L WSe_2, further supporting the idea that the self-limiting nature of the SLS process is layer dependent.

For further examination of SLS MoS_2 on WSe_2, Raman mapping of the MoS_2 E^1_{2g} peak intensity and position was compared against OM images of 1L SLS MoS_2 grown on WSe_2 flakes on a SiO_2 substrate. In Fig. 3(d), regions confirmed by Raman analysis and AFM (See Supplementary Fig. S8(d)) to be 2L WSe_2 are indicated by white arrows, with the rest being bulk WSe_2. The Raman map of MoS_2 E^1_{2g} intensity in Fig. 3(e) shows that a strong MoS_2 E^1_{2g} signal is observed only at 2L WSe_2 regions, indicating that MoS_2 was not synthesized on bulk WSe_2. The Raman map of MoS_2 E^1_{2g} position (Fig. 3(f)) further supports the notion that MoS_2 grows only on 2L WSe_2, which is accompanied by a downshift relative to the MoS_2 E^1_{2g} position on SiO_2. This confirms the validity of using SLS to produce MoS_2 on other chemically inert surfaces such as WSe_2, and indicates that the process has the potential for widespread application.

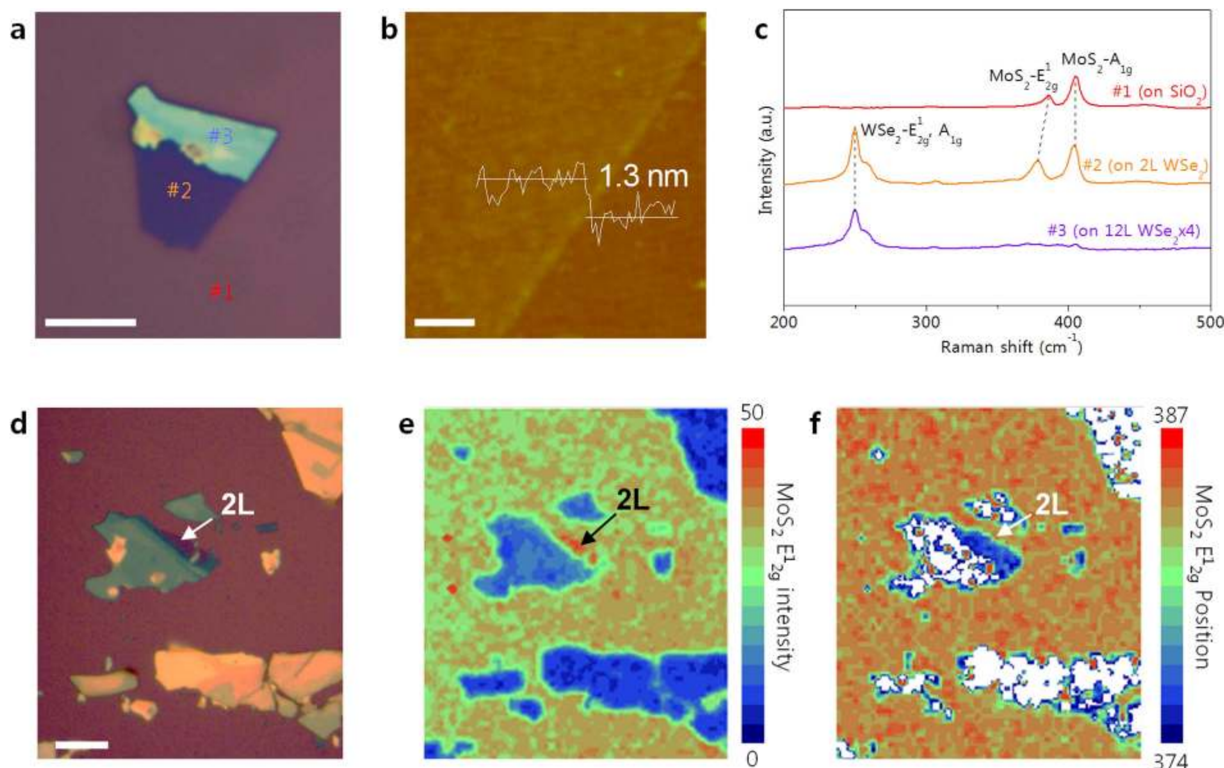

Figure 3. (**a**) OM image of an exfoliated WSe_2 flake on SiO_2 (scale bar = 10 μm). (**b**) AFM image and height profile of SLS MoS_2 on 2L WSe_2 region (scale bar = 0.5 μm). (**c**) Raman spectra for the numbered regions in Figure 3(a): #1: MoS_2 on SiO_2, #2: MoS_2 on 2L WSe_2 and #3L SLS MoS_2 on 12L WSe_2. (**d**) OM image of SLS MoS_2 on exfoliated WSe_2 flakes (scale bar = 10 μm) and corresponding Raman mapping results for (**e**) MoS_2 E^1_{2g} intensity and (**f**) MoS_2 E^1_{2g} position.

As the SLS process clearly allows for much greater layer control than previously reported methods[10,42,43], it represents a promising option for fabricating atomically thin functional devices such as PN diodes, light emitting diodes and inverters[10,12,44]. To test this, a PN diode was fabricated using a 1L SLS MoS_2/2L WSe_2 heterostructure, with Fig. 4(a,b) showing the device structure and an OM image of the fabricated PN diode. Operation of this device is dependent on the back gate voltage, which as shown in Fig. 4(c), can be adjusted by varying the carrier concentration through electrical doping. In other words, the PN diode exhibits a gate-tunable characteristic, with an increase in gate voltage from -60 to 20 V changing the p-n rectifying configuration to n-n junction behavior. The calculated forward/reverse current ratio at $V_{ds} = |5\,V|$ clearly shows this gate-tunable PN diode characteristic (inset of Fig. 4(c)). The forward/reverse current ratio of ~80 at $V_g = -60$ V, is higher than previously reported for a PN diode based on 1L MoS_2/1L WSe_2 (~50 at $V_{ds} = |8|V)$[45], but drops to 1.4 at $V_g = 20$ V. This gate-tunable characteristic could be explained by a variation in carrier density with electrical doping, as consistent with a previous report[45] (also explain in Supplementary Fig. S10). Also of note is the fact that this PN diode exhibits a strong PL quenching property and photovoltaic effect, indicating a rapid carrier separation at the MoS_2/WSe_2 junction[10,42]. Figure 4(d) shows the PL spectra for 1L MoS_2, 2L WSe_2 and the heterostructure created from them. It is evident from this that the strong PL peak for the direct gap transition of 1L MoS_2 is greatly suppressed by the WSe_2 junction, which is attributed to the rapid separation of charge carriers[10]. Figure 4(e) shows the I-V characteristics of a MoS_2/WSe_2 PN diode at Vg = -50 V with and without illumination by an incident optical power density of 14 W/m^2. We see from this that the current increases with illumination due to the generation of optically excited carriers. The open circuit voltage of 0.2 V indicates a photovoltaic effect, with a calculated photoresponsivity of 33 mA/W at $V_{ds} = 1$ V. As a result, we show the potential of SLS MoS_2/WSe_2 structure in photovoltaic device as well as PN diode.

Conclusion

In summary, the synthesis of MoS_2 on a SiO_2 substrate has been successfully achieved through a new self-limiting process that allows the number of layers formed to be controlled by varying the growth temperature. Though the precise mechanism requires further study, this behavior is believed to be caused by the lack of dangling bonds on the surface of MoS_2 and the screening effect that MoS_2 layers have on the substrate's electric field. More importantly, this process can achieve excellent layer uniformity (up to 95%) over large areas at wafer-level scale. The resulting 2D MoS_2 can produce n-type behavior and a high on/off ratio when used in a top-gated FET, and can be grown on other chemically inert 2D materials such as WSe_2. Indeed, a PN diode based on a MoS_2/WSe_2 heterostructure is capable of a high forward/reverse current ratio, and exhibits a gate-tunable rectifying property attributable to

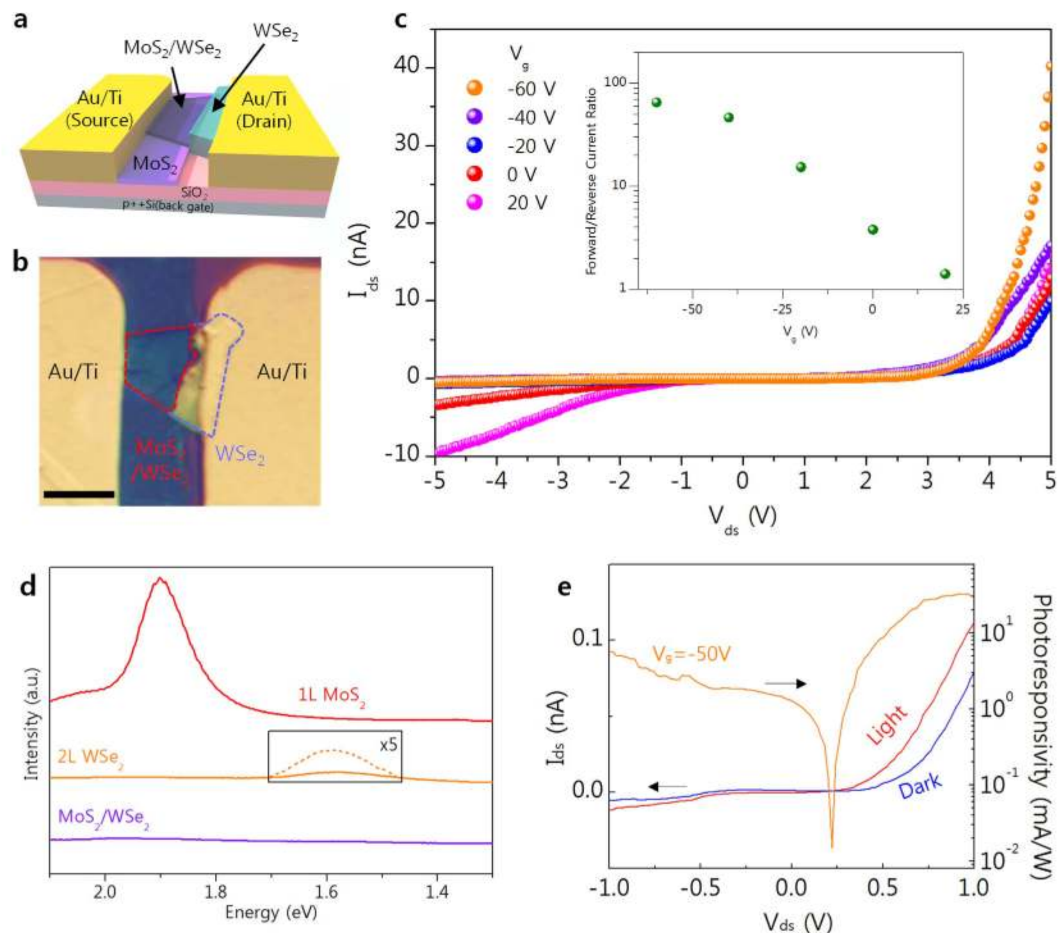

Figure 4. (**a**) Schematic and (**b**) OM image of fabricated PN diode. (**c**) I–V characteristics of PN diode with various gate bias values of between −60 and 20 V, and (inset) forward/reverse current ratio at $V_{ds} = |5\,V|$. (**d**) PL spectra for 1L MoS_2 (red) 2L WSe_2 (orange) and a heterostructure created by the two (violet). (**e**) I–V characteristics with (red) and without illumination (blue), and calculated photoresponsivity (orange).

electrical doping by gate voltage. We therefore believe that this new method could be extended to the development of other 2D TMDCs materials and 2D heterostructures.

Methods

SLS MoS_2 Growth. A tube furnace reactor was used to synthesize MoS_2 directly onto SiO_2 (285 nm)/Si substrates using $MoCl_5$ and H_2S as the precursor and reactant, respectively. A bubbler containing the precursor was heated to 90 °C to ensure an adequate vapor pressure for the precursor molecules to be carried into the tube by pure argon (99.999%) carrier gas. The SLS cycle consisted of four steps, each with the same with ALD procedure of: precursor exposure for 4 s, a 5s Ar purge, 3 s H_2S reactant exposure, and a final 5 s Ar purge.

Transfer of MoS_2. The as-synthesized MoS_2 on the SiO_2 substrate was spin coated with polymethyl methacrylate (PMMA) at 4000 rpm for 60 s. After curing the PMMA at 100 °C for 15 min, the sample was immersed in a 10% HF solution to etch away the SiO_2 layer. The sample was then washed with DI water and transferred to a new SiO_2/Si substrate. Finally, the PMMA was removed using acetone and the sample washed with isopropyl alcohol.

Fabrication of Top-Gated Field-Effect Transistor. The MoS_2-based FET was fabricated from as-synthesized 1L MoS_2 on a SiO_2 (300 nm)/Si substrate by evaporating Au(10 nm)/Ti(50 nm) electrodes and an ALD Al_2O_3 (40nm) gate insulator through conventional photolithography and reactive ion (O_2plasma) etching.

Fabrication of PN diode. The 1L SLS MoS_2 was synthesized on WSe_2 flakes at 800 °C. Then, PN diode was fabricated from an SLS MoS_2/WSe_2 heterostructure on a SiO_2 (300 nm)/Si substrate by evaporating Au(10 nm)/Ti(50 nm) electrodes. After etching, electrical contacts were formed between the drain electrode and 12L WSe_2, and between the MoS_2 and source electrode.

Characterization of MoS_2. OM (Nikon ECLIPSE LV100ND), SEM(JEOL-6701F), Raman spectroscopy (HORIBA, Lab Ram ARAMIS; 532 nm laser excitation wavelength), AFM (VEECO, Multimode), PL (SPEX1403, SPEX; 532 nm laser excitation wavelength), XPS (Thermo U.K., K-alpha radiation), TEM (FEI Titan G2 Cube

60-300, accelerating voltage = 80 kV) and a voltage/current meter (Keithley 4200, Keithley Instruments) were all used in characterizing the SLS MoS_2 nanosheets.

References

1. Geim, A. K. & Novoselov, K. S. The rise of graphene. *Nature Mater*. **6,** 183–191 (2007).
2. Novoselov, K. *et al.* Two-dimensional atomic crystals. *Proc. Natl Acad. Sci.USA*. **102,** 10451–10453 (2005).
3. Fiori, G. *et al.* Electronics based on two-dimensional materials. *Nature Nanotech*. **9,** 768–779 (2014).
4. Xia, F., Wang, H., Xiao, D., Dubey, M. & Ramasubramaniam, A. Two-dimensional material nanophotonics. *Nature Photon*. **8,** 899–907 (2014).
5. Xu, M., Liang, T., Shi, M. & Chen, H. Graphene-like two-dimensional materials. *Chem Rev.* **113,** 3766–3798 (2013).
6. Kim, K. S. *et al.* Large-scale pattern growth of graphene films for stretchable transparent electrodes. *Nature*. **457,** 706–710 (2009).
7. Bae, S. *et al.* Roll-to-roll production of 30-inch graphene films for transparent electrodes. *Nature Nanotech*. **5,** 574–578 (2010).
8. Li, X. *et al.* Large-area synthesis of high-quality and uniform graphene films on copper foils. *Science*. **324,** 1312–1314 (2009).
9. Wu, W. *et al.* Piezoelectricity of single-atomic-layer MoS2 for energy conversion and piezotronics. *Nature*. **514,** 470–474 (2014).
10. Lee, C.-H. *et al.* Atomically thin p–n junctions with van der Waals heterointerfaces. *Nature Nanotech*. **9,** 676–681 (2014).
11. Georgiou, T. *et al.* Vertical field-effect transistor based on graphene-WS2 heterostructures for flexible and transparent electronics. *Nature Nanotech*. **8,** 100–103 (2013).
12. Withers, F. *et al.* Light-emitting diodes by band-structure engineering in van der Waals heterostructures. *Nature Mater*. **14,** 301–306 (2015).
13. Shi, H. *et al.* Exciton dynamics in suspended monolayer and few-layer MoS_2 2D crystals. *ACS Nano*. **7,** 1072–1080 (2013).
14. Lee, H. S. *et al.* MoS2 Nanosheet Phototransistors with Thickness-Modulated Optical Energy Gap. *Nano Lett*. **12,** 3695–3700 (2012).
15. Song, J.-G. *et al.* Layer-Controlled, Wafer-Scale, and Conformal Synthesis of Tungsten Disulfide Nanosheets Using Atomic Layer Deposition. *ACS Nano*. **7,** 11333–11340, (2013).
16. Lee, Y. *et al.* Synthesis of Large-Area MoS_2 Atomic Layers with Chemical Vapor Deposition. *Adv. Mater.* **24,** 2320–2325 (2012).
17. Lin, Y. *et al.* Wafer-scale MoS_2 thin layers prepared by MoO_3 sulfurization. *Nanoscale*. **4,** 6637–6641 (2012)
18. Shi, Y., Li, H. & Li, L.-J. Recent advances in controlled synthesis of two-dimensional transition metal dichalcogenides via vapour deposition techniques. *Chem Soc Rev*. **44,** 2744–2756 (2015).
19. Kim, H., Lee, H.-B.-R. & Maeng, W. J. Applications of atomic layer deposition to nanofabrication and emerging nanodevices. *Thin Solid Films* **517,** 2563–2580 (2009).
20. Hyungjun, K. Characteristics and applications of plasma enhanced-atomic layer deposition. *Thin Solid Films* **519,** 6639–6644 (2011).
21. Tan, L. K. *et al.* Atomic layer deposition of a MoS_2 film. *Nanoscale*. **6,** 10584–10588 (2014).
22. Jin, Z., Shin, S., Kwon, D. H., Han, S.-J. & Min, Y.-S. Novel chemical route for atomic layer deposition of MoS 2 thin film on SiO 2/Si substrate. *Nanoscale.* **6,** 14453–14458 (2014).
23. Hara, S. *et al.* Self-limiting growth on the β-SiC(001) surface. *Surf. Sci*. **273,** 437–441 (1992).
24. Elam, J. W., Nelson, C. E., Grubbs, R. K. & George, S. M. Nucleation and growth during tungsten atomic layer deposition on SiO2 surfaces. *Thin Solid Films*. **386,** 41–52 (2001).
25. Jung, H. *et al.* Fabrication of Transferable Al2O3 Nanosheet by Atomic Layer Deposition for Graphene FET. *ACS Appl. Mater. Interfaces*. **6,** 2764–2769 (2014).
26. Kim, K. *et al.* Selective metal deposition at graphene line defects by atomic layer deposition. *Nature Commun*. **5,** 4781 (2014).
27. Lee, H.-B.-R., Baeck, S. H., Jaramillo, T. F. & Bent, S. F. Growth of Pt Nanowires by Atomic Layer Deposition on Highly Ordered Pyrolytic Graphite. *Nano Lett*. **13,** 457–463 (2013).
28. McDonnell, S. *et al.* HfO2 on MoS2 by Atomic Layer Deposition: Adsorption Mechanisms and Thickness Scalability. *ACS Nano* **7,** 10354–10361 (2013).
29. Yu, Y. *et al.* Controlled Scalable Synthesis of Uniform, High-Quality Monolayer and Few-layer MoS2 Films. *Sci. Rep.* **3,** 1866 (2013).
30. Li, S.-L. *et al.* Quantitative Raman Spectrum and Reliable Thickness Identification for Atomic Layers on Insulating Substrates. *ACS Nano* **6,** 7381–7388 (2012).
31. Li, H. *et al.* From bulk to monolayer MoS2: evolution of Raman scattering. *Adv. Funct. Mater.* **22,** 1385–1390 (2012).
32. Ling, X. *et al.* Role of the Seeding Promoter in MoS2 Growth by Chemical Vapor Deposition. *Nano Lett.* **14,** 464–472 (2014).
33. Schmidt, H. *et al.* Transport Properties of Monolayer MoS2 Grown by Chemical Vapor Deposition. *Nano Lett.* **14,** 1909–1913 (2014).
34. Eda, G. *et al.* Photoluminescence from Chemically Exfoliated MoS2. *Nano Lett.* **11,** 5111–5116 (2011).
35. Mak, K. F., Lee, C., Hone, J., Shan, J. & Heinz, T. F. Atomically Thin MoS_ {2}: A New Direct-Gap Semiconductor. *Phys. Rev. Lett.* **105,** 136805 (2010).
36. Liu, H., Xu, K., Zhang, X. & Peide, D. Y. The integration of high-k dielectric on two-dimensional crystals by atomic layer deposition. *Appl. Phys. Lett.* **100,** 152115 (2012).
37. Castellanos-Gomez, A.*et al.* Electric-Field Screening in Atomically Thin Layers of MoS2: the Role of Interlayer Coupling. *Adv. Mater.* **25,** 899–903 (2013).
38. Wang, M. *et al.* Catalytic Transparency of Hexagonal Boron Nitride on Cu for Chemical Vapor Deposition Growth of Large Area and High Quality Graphene. *ACS Nano*. **8,** 5478–5483 (2014).
39. Radisavljevic, B., Radenovic, A., Brivio, J., Giacometti, V. & Kis, A. Single-layer MoS2 transistors. *Nature Nanotech*. **6,** 147–150 (2011).
40. Bhatt, S. V., Deshpande, M., Sathe, V., Rao, R. & Chaki, S. Raman spectroscopic investigations on transition-metal dichalcogenides MX2 (M = Mo, W; X = S, Se) at high pressures and low temperature. *J. Raman Spectrosc.* **45,** 971–979 (2014).
41. Chiu, M.-H. *et al.* Spectroscopic Signatures for Interlayer Coupling in MoS2-WSe2 van der Waals Stacking. *ACS Nano*. **8,** 9649–9656 (2014).
42. Fang, H. *et al.* Strong interlayer coupling in van der Waals heterostructures built from single-layer chalcogenides. *Proc. Natl Acad. Sci.USA*. **111,** 6198–6202 (2014).
43. Gong, Y. *et al.* Vertical and in-plane heterostructures from WS2/MoS2 monolayers. *Nature Mater*. **13,** 1135–1142 (2014).
44. Duan, X. *et al.* Lateral epitaxial growth of two-dimensional layered semiconductor heterojunctions. *Nature Nanotech*. **9,** 1024–1030 (2014).
45. Furchi, M. M., Pospischil, A., Libisch, F., Burgdörfer, J. & Mueller, T. Photovoltaic effect in an electrically tunable van der Waals heterojunction. *Nano Lett*. **14,** 4785–4791 (2014).

Acknowledgements

This work was supported by the Center for Integrated Smart Sensors funded by the Ministry of Science, ICT & Future Planning as Global Frontier Project (CISS-2011-0031848); This work was supported by Korea Evaluation Institute of Industrial Technology (KEIT) funded by the Ministry of Trade, Industry and Energy (MOTIE) (Project No. 10050296, Large scale (Over 8") synthesis and evaluation technology of 2-dimensional chalcogenides for next generation electronic devices); This work was supported by Samsung Display Co., Ltd.; and a National Research Foundation of Korea (NRF) grant funded by the Korea government (MSIP) (No. NRF-2014R1A2A1A11052588).

Author Contributions

Y.K. and J.-G.S. contributed equally to this work. Y.K. and J.-G.S. carried out most experiments and analyzed the data. Y.J.P., W.J.W. and J.-H.A. made the FET devices and carried out the electrical measurement. G.H.R. and Z.L. contributed to TEM measurement. S.J.L.and J.-M.M. performed PL characterization. J.S.K., P.J.J., W.J.W. and S.I. contributed to fabrication of PN diode. T.C. and H.J. contributed to AFM and SEM measurement. C.W.L. and J.P. contributed to XPS measurement and analysis data. Y.K., J.-G.S., H.L., J.P. and H.K. designed the experiment and co-wrote the paper. All of the authors discussed the results and commented on the paper.

Additional Information

Supplementary information accompanies this paper at http://www.nature.com/srep

Competing financial interests: The authors declare no competing financial interests.

How to cite this article: Kim, Y. *et al.* Self-Limiting Layer Synthesis of Transition Metal Dichalcogenides. *Sci. Rep.* **6**, 18754; doi: 10.1038/srep18754 (2016).

This work is licensed under a Creative Commons Attribution 4.0 International License. The images or other third party material in this article are included in the article's Creative Commons license, unless indicated otherwise in the credit line; if the material is not included under the Creative Commons license, users will need to obtain permission from the license holder to reproduce the material. To view a copy of this license, visit http://creativecommons.org/licenses/by/4.0/